Optics Letters

Multi-foci metalens for terahertz polarization detection

Ruoxing Wang,[1,2] Jin Han,[2,3] Jianlong Liu,[1,4] Hao Tian,[4] Weimin Sun,[1] Li Li,[1,5] and Xianzhong Chen[2,6]

[1]Key Laboratory of In-Fiber Integrated Optics of Ministry of Education, Harbin Engineering University, Harbin 150001, China
[2]Institute of Photonics and Quantum Sciences, School of Engineering and Physical Sciences, Heriot-Watt University, Edinburgh EH14 4AS, UK
[3]College of Material Science and Engineering, Kunming University of Science and Technology, Kunming 650093, China
[4]Department of Physics, Harbin Institute of Technology, Harbin 150001, China
[5]e-mail: lylee_heu@hrbeu.edu.cn
[6]e-mail: x.chen@hw.ac.uk

Received 20 April 2020; revised 18 May 2020; accepted 21 May 2020; posted 26 May 2020 (Doc. ID 395580); published 23 June 2020

We propose a reflective terahertz (THz) metalens with four focal points for polarization detection of THz beams. The metalens is composed of *Z*-shaped resonators with spatially variant orientations, a reflective gold layer, and a dielectric spacer between them. The polarization states of the focal points include left circular polarization, right circular polarization, an incident polarization state, and a polarization state whose major axis is rotated $\pi/4$ in comparison with that of the incident polarization. The handedness, ellipticity, and major axis of the polarization state can be determined based on the light intensities of the focal points. The uniqueness of the designed device renders this technique very attractive for applications in compact THz polarization detection and information processing.

https://doi.org/10.1364/OL.395580

Conventional optical components rely on the accumulated phase delay during light propagation to shape light beams, leading to bulky optical components and large volume of the imaging systems, which are not suitable for device miniaturization and system integration. Recently, the emerging metasurfaces, known as 2D metamaterials, can manipulate light's amplitude, phase, and polarization at subwavelength resolution [1,2], which provides a new platform to develop a plethora of ultrathin optical elements in various research fields, including holograms [3,4], focusing [5–9], polarization measurement [10,11], vortex beam generation [12,13] and others [14,15].

The function of a conventional lens is typically fixed, which restricts the development of on-chip optical integration. Benefitting from the exotic properties of metasurfaces, a variety of metalenses with unusual functions have been proposed, including the dual-polarity plasmonic metalens [5], multi-foci metalens [16,17], metalens array [18,19], broadband achromatic metalens [7,8], aplanatic metalens [9], asymmetric metalens [20], multifunctional metalens with integrated polarization rotation or holography, and others [21–23]. Most materials in the terahertz (THz) range have properties quite different from those they possess in the visible range. As one of the fundamental components, a THz lens plays an important role in various systems [24,25]. Although there have been efforts to develop metalenses in the THz regime recently [20,24–33], these are still insufficient compared with the studies on the metalens in the visible range. Ultrathin multifunctional THz lenses are desirable for the development of compact THz systems for THz polarization detection and imaging [24–27].

A traditional THz polarization detection system includes many optical components such as polarizers, wave plates, and polarization modulators, resulting in large volume and unfavorable integration. To tackle this technical challenge, some efforts have been made on a spin-selective THz metalens [25,28,29]. They are sensitive to left circular polarization (LCP) or right circular polarization (RCP). However, a THz metalens with multiple focal points for polarization detection has not been reported. Here we report on a THz multi-foci metalens that can be used to determine the handedness, ellipticity, and major axis of an incident state. We propose an ultrathin reflective THz metalens with four focal points that consist of *Z*-shaped resonators with spatially variant orientations, a reflective gold layer, and a dielectric spacer sandwiched between them. Unlike previously reported multi-foci metalenses, our multi-foci metalens can simultaneously separate circular polarization states and realize polarization rotation functionality in the same focal plane. The polarization information of the THz beam is obtained based on the intensities of the focal points. The ultrathin and compact features render the designed device very attractive for THz polarization detection and information processing.

The schematic of the multi-foci metalens for a THz incident beam with the ellipticity angle χ and the major axis direction β is shown in Fig. 1. The relationship between the ellipticity angle χ and the ellipticity η is described by $\chi = \arctan(\eta)$.

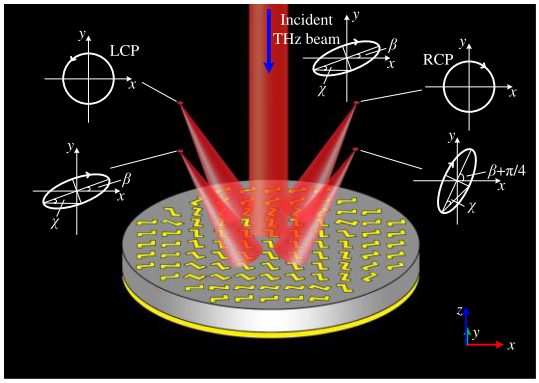

Fig. 1. Schematic of the reflective THz multi-foci metalens for polarization detection. The ellipticity angle χ and the direction of the major axis β of the incident and reflected polarization states are indicated in polarization ellipses.

The beam is reflected and focused at four points in space by the metalens. The polarization state in each focal point is different. The polarization states of the focal points include LCP, RCP, an incident polarization state, and a polarization state whose major axis is rotated $\pi/4$ in comparison with that of the incident polarization. The intensities of LCP and RCP focal points can be used to determine the handedness and the ellipticity of the incident polarization state, while the intensities of the other two focal points can be used to determine the major axis of the incident polarization state.

The designed multi-foci metalens consists of gold Z-shaped resonators with different orientations sitting on a polyimide layer in the middle and a gold layer at the bottom. It has been reported that this structure has a high circular polarization conversion efficiency in the telecomband [34], as well as in the THz regime based on our calculation. Each unit cell has a period $p = 100$ μm. The parameters of gold resonators include $l = 75$ μm, $w = 20$ μm, and the thickness $h_1 = 150$ nm. The polyimide spacer thickness is $h_2 = 30$ μm, and the reflective gold layer thickness is $h_3 = 150$ nm. The detailed information is given in the inset of Fig. 2. The electrical conductivity of gold and the complex permittivity of the polyimide from the reference [35] are $\sigma_g = 4.561 \times 10^7$ S/m and $\varepsilon_p = 3.5 + 0.035$i, respectively. With these geometric parameters, the simulated circular polarization conversion ratio (PCR) of the metalens is shown in Fig. 2, which is calculated by using the frequency domain solver of the Computer Simulation Technology Microwave Studio software. In the simulation, a unit cell boundary is used along the x and y directions, and the open boundary is used along the z direction. The PCR is defined as $\mathrm{PCR} = R_{\mathrm{cross}}/(R_{\mathrm{co}} + R_{\mathrm{cross}})$, where R_{co} and R_{cross} represent the reflectivity of unconverted and converted THz beams, respectively [36]. From Fig. 2, we can see that the PCR is higher than 90% at a broadband from 0.97 to 1.69 THz, and the energy loss rate is less than 15%. We choose to design the metalens at 1.15 THz (corresponding to $\lambda = 260.87$ μm). At this operating frequency, the PCR is as high as 99.8%, and the energy loss rate is only 6.5%. The total thickness of the designed metalens is 30.3 μm, only about 1/9 of the operating wavelength.

The phase profiles of the lenses to achieve the four off-axis focal positions are governed by the following Eqs. (1)–(4):

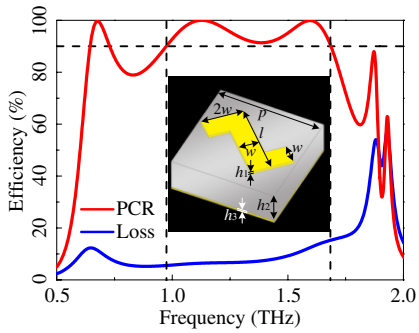

Fig. 2. Simulated PCR and energy loss rate based on the unit cell (inset) for the incident beam at normal incidence.

$$\phi_1(x, y) = -\frac{2\pi}{\lambda}\left(\sqrt{f^2 + (x+a)^2 + (y-a)^2} - f_D\right), \quad (1)$$

$$\phi_2(x, y) = -\frac{2\pi}{\lambda}\left(\sqrt{f^2 + (x-a)^2 + (y-a)^2} - f_D\right), \quad (2)$$

$$\phi_3(x, y) = -\frac{2\pi}{\lambda}\left(\sqrt{f^2 + (x+a)^2 + (y+a)^2} - f_D\right), \quad (3)$$

$$\phi_4(x, y) = -\frac{2\pi}{\lambda}\left(\sqrt{f^2 + (x-a)^2 + (y+a)^2} - f_D\right), \quad (4)$$

where $f_D = \sqrt{f^2 + 2a^2}$, $a = 1$ mm determines the positions of focal points, and the designed focal plane is located at $f = 5$ mm.

Our designed metalens is implemented by using a Pancharatnam-Berry phase generated by the geometric metasurface; thus, the phase profiles in Eqs. (1)–(4) can only converge the incident LCP beam and diverge RCP beam. To achieve the envisaged design, the phase profiles of four metalenses need to be modified as Eqs. (5)–(8)

$$\varphi_1(x, y) = \phi_1(x, y), \quad (5)$$

$$\varphi_2(x, y) = -\phi_2(x, y), \quad (6)$$

$$\varphi_3(x, y) = \arg\{e^{i[\phi_3(x,y)]} + e^{i[-\phi_3(x,y)]}\}, \quad (7)$$

$$\varphi_4(x, y) = \arg\{e^{i[\phi_4(x,y)+\pi/4]} + e^{i[-\phi_4(x,y)+\pi/4]}\}. \quad (8)$$

Because the first focal point only converges with the LCP beam, the phase profile in Eq. (1) remains unchanged, as shown in Eq. (5). The second focal point only converges with the RCP beam, so the phase profile in Eq. (2) should become negative, as shown in Eq. (6). The third and the fourth focal points can converge LCP and RCP simultaneously. Thus, Eqs. (7) and (8) need to contain the terms that converge with LCP and RCP at the same time. However, this also means that the convergent term of one circular polarization is the divergent term of the opposite circular polarization. Therefore, the theoretical focusing efficiency cannot exceed 50% for the two foci. Additionally, for the fourth focal point, a rotation angle of polarization major axis is introduced, as shown in Eq. (8), to achieve the rotation of the major axis of the incident polarization state [20,21].

The total phase profile of the designed multi-foci metalens can be described as [17,29]

$$\Phi(x, y) = \arg\left(\sum_{j=1}^{4} e^{i\varphi_j(x,y)}\right). \tag{9}$$

By using the phase profile in Eq. (9), the four focal points with predesigned functions can be achieved. Each Z-shaped resonator in location (x, y) is rotated counterclockwise with an angle of $\Phi(x, y)/2$, which is based on the geometric metasurface [4].

A completely polarized THz beam can be decomposed into LCP and RCP components. The intensity ratio τ of LCP and RCP components can deduce the ellipticity and the handedness of the polarized light. The ellipticity is written as

$$\eta = (1 - \sqrt{\tau})/(1+\sqrt{\tau}). \tag{10}$$

$\eta = \pm 1$ and $\eta = 0$ represent RCP(LCP) and linear polarization (LP), $-1 < \eta < 0$ represents left-handed elliptical polarization (LEP), and $0 < \eta < 1$ represents right-handed elliptical polarization (REP) [37]. According to the characteristics of the metalens we designed, the polarization states of the first and the second foci are LCP and RCP, respectively. Thus, the ratio of the intensity of the first focal point (I_1) to that of the second focal point (I_2) is the ellipticity of the incident THz beam. Here all the simulated normalized intensity distributions at the focal plane are calculated based on the Fresnel-Kirchhoff diffraction integral [38]. When the incident THz beam is LCP, the converted LCP converges at the first focal point, and there is no RCP that is converted from the incident beam converging at the second focal point. The normalized intensity distribution at the focal plane is shown in Fig. 3(a). The normalized intensity at the first focal point $I_1 = 0.957$, and the normalized intensity at the second focal point $I_2 = 4.73 \times 10^{-4}$. The calculated ellipticity $\eta = -0.9565$. (The theoretical value is -1.) The slight difference between simulation and theory is mainly due to the discretization of the Fresnel-Kirchhoff diffraction integral. When the incident THz beam changes to RCP, there is no LCP component from the incident beam that can be converged at the first focal point, and the RCP part is converged at the second focal point. At this moment, $I_1 = 7.88 \times 10^{-4}$ and $I_2 = 0.9967$, as shown in Fig. 3(b). The calculated ellipticity $\eta = 0.9453$ (theoretical value is 1). The ellipticity with 99.9% component RCP(LCP) and 0.1% component LCP(RCP) is ± 0.9387. Thus, we can infer that according to Figs. 3(a) and 3(b), the incident polarization states are LCP and RCR, respectively, with an error less than 0.1%. When the incident polarization states, respectively, are LEP ($\eta = -0.5$), LP ($\eta = 0$) and REP ($\eta = 0.268$), the normalized intensity distributions at the focal plane are shown in Figs. 3(c)–3(e). The calculated ellipticities of polarization are (c) $\eta = -0.4915$, (d) $\eta = 0.0101$, and (e) $\eta = 0.2768$, based on the intensity distributions (c) $I_1 = 0.861$, $I_2 = 0.100$; (d) $I_1 = 0.479$, $I_2 = 0.499$; and (e) $I_1 = 0.240$, $I_2 = 0.748$, respectively. The maximum deviation of the ellipticity from the theoretical value is only about 0.01. Therefore, it can be considered that our designed metalens can be used to detect the handedness and the ellipticity of the incident beam. So far, we have not considered the intensities at the third focal point (I_3) and the fourth focal point (I_4). It is because they converge half of LCP and half of RCP, and diverge the other half of LCP and RCP. The theoretical intensities are always 0.5, regardless of the ellipticity of the polarized beam.

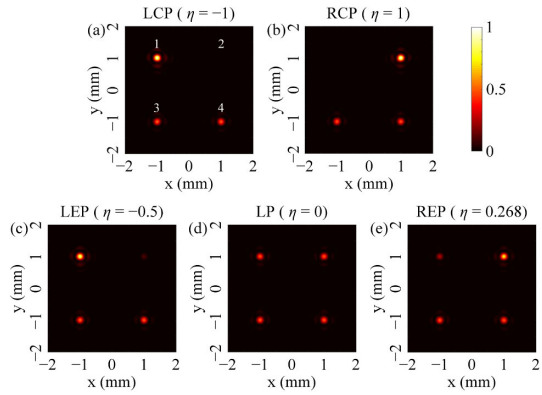

Fig. 3. Simulated normalized intensity distributions at the focal plane upon the illumination of the incident THz beam with (a) LCP($\eta = -1$), (b) RCP($\eta = 1$), (c) LEP($\eta = -0.5$), (d) LP($\eta = 0$), and (e) REP($\eta = 0.268$).

When the ellipticity and the handedness of the incident THz beam can be confirmed by intensities I_1 and I_2, we can further determine the major axis direction by the intensities I_3 and I_4 with a polarizer. This is because the major axis direction at the third focal point is the same as the incident major axis direction, and the major axis direction at the fourth focal point is rotated counterclockwise by $\pi/4$ with respect to the incident beam. Place a polarizer in front of the third focal point and the fourth focal point, and the intensities I_3 and I_4 will change. The transmission axis of the polarizer is fixed along the horizontal direction, the relationship between the incident major axis direction, and the normalized intensities I_3 and I_4 are shown in Fig. 4(a). After I_3 and I_4 are obtained, the incident major axis direction can be analyzed. A single value of I_3 corresponds to two possible major axis directions [see Fig. 4(a)]. Similarly, a single value of I_4 also corresponds to two possible major axis directions, but only one is the same as that determined by I_3, which is the major axis direction of the incident polarization state. Figures 4(b)–4(e) present the normalized intensity distributions at the focal plane after passing through the polarizer. When the incident LP directions are 0 and $\pi/4$, as shown in Figs. 4(b) and 4(c), the calculated polarization direction deviations θ_d from the incident polarization direction are (b) $\theta_d = -0.015\pi$ and (c) $\theta_d = 0.001\pi$, based on the obtained intensity distributions (b) $I_3 = 0.494$, $I_4 = 0.244$ and (c) $I_3 = 0.247$, $I_4 = 1.83 \times 10^{-33}$, respectively. From Figs. 4(d) and 4(e), we can obtain the normalized intensities (d) $I_1 = 0.718$, $I_2 = 0.250$, $I_3 = 1.86 \times 10^{-33}$, $I_4 = 0.243$ and (e) $I_1 = 0.096$, $I_2 = 0.897$, $I_3 = 0.368$, $I_4 = 0.459$, respectively. Based on the intensity distributions, we can infer that the incident beam is LEP with ellipticity $\eta = -0.2582$ and major axis direction $\beta = 0.498\pi$ in Fig. 4(d). The deviation of the ellipticity is 0.01, and the major axis direction deviation is $\theta_d = -0.002\pi$. Additionally, we can infer that the incident beam is REP with ellipticity $\eta = 0.5062$ and major axis direction $\beta = 0.835\pi$ in Fig. 4(e). The ellipticity deviation is only 0.006; the major axis direction deviation is $\theta_d = 0.002\pi$. The maximum deviation of the major axis direction is only 0.015π in Fig. 4. Thus, our designed metalens is effective for measuring the major axis direction of an incident THz beam. With the ellipticity η and the major axis direction β of the incident

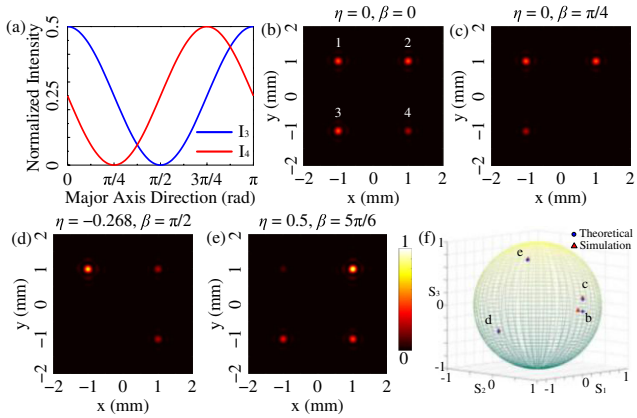

Fig. 4. (a) Relationship between the incident major axis direction and the normalized intensities I_3 and I_4 with a polarizer with a transmission axis fixed along the horizontal direction, which is placed in front of the third focal point and the fourth focal point. (b)–(e) Simulated normalized intensity distributions at the focal plane after passing through the polarizer. The ellipticities and the major axis direction of the incident polarization states are (b) 0, 0; (c) 0, $\pi/4$; (d) -0.268, $\pi/2$; and (e) 0.5, $5\pi/6$, respectively. (f) Poincaré sphere to show the polarization states in (b)–(e).

polarization state, its normalized Stokes parameters ($S_0 = 1$) can be calculated by $S_1 = \cos 2\chi \cos 2\beta$, $S_2 = \cos 2\chi \sin 2\beta$, $S_3 = \sin 2\chi$, where $\chi = \arctan(\eta)$ [37]. The polarization states in Figs. 4(b)–4(e) are shown on the Poincaré sphere in Fig. 4(f).

In summary, we have proposed an ultrathin reflective THz metalens with four focal points for polarization measurement. The unique property of the designed THz metalens lies in the polarization difference in each focal point, which can be used to determine the handedness, ellipticity, and the major axis of the incident polarization state of a THz beam. The deviation between the simulation result and the theoretical value is within an acceptable level. Combined with its ultrathin and compact features, our designed metalens is very attractive in the field of THz polarization detection and information processing.

Funding. Natural Science Foundation of Heilongjiang (LH2019F012); Engineering and Physical Sciences Research Council (EP/P029892/1); 111 project to Harbin Engineering University (B13015); China Scholarship Council (201808535073, 201906680066).

Disclosures. The authors declare no conflicts of interest.

REFERENCES

1. N. Yu, P. Genevet, M. A. Kats, F. Aieta, J. P. Tetienne, F. Capasso, and Z. Gaburro, Science **334**, 333 (2011).
2. D. Lin, P. Fan, E. Hasman, and M. L. Brongersma, Science **345**, 298 (2014).
3. G. Zheng, H. Mühlenbernd, M. Kenney, G. Li, T. Zentgraf, and S. Zhang, Nat. Nanotechnol. **10**, 308 (2015).
4. D. Wen, F. Yue, G. Li, G. Zheng, K. Chan, S. Chen, M. Chen, K. F. Li, P. W. H. Wong, K. W. Cheah, E. Y. B. Pun, S. Zhang, and X. Chen, Nat. Commun. **6**, 8241 (2015).
5. X. Chen, L. Huang, H. Mühlenbernd, G. Li, B. Bai, Q. Tan, G. Jin, C. Qiu, S. Zhang, and T. Zentgraf, Nat. Commun. **3**, 1198 (2012).
6. X. Ni, S. Ishii, A. V. Kildishev, and V. M. Shalaev, Light Sci. Appl. **2**, e72 (2013).
7. S. Wang, P. C. Wu, V. C. Su, Y. C. Lai, M. K. Chen, H. Y. Kuo, B. H. Chen, Y. H. Chen, T. T. Huang, J. H. Wang, R. M. Lin, C. H. Kuan, T. Li, Z. Wang, S. Zhu, and D. P. Tsai, Nat. Nanotechnol. **13**, 227 (2018).
8. W. T. Chen, A. Y. Zhu, V. Sanjeev, M. Khorasaninejad, Z. Shi, E. Lee, and F. Capasso, Nat. Nanotechnol. **13**, 220 (2018).
9. C. Chen, W. Song, J. W. Chen, J. H. Wang, Y. H. Chen, B. Xu, M. K. Chen, H. Li, B. Fang, J. Chen, H. Y. Kuo, S. Wang, D. P. Tsai, S. Zhu, and T. Li, Light Sci. Appl. **8**, 99 (2019).
10. X. Zhang, S. Yang, W. Yue, Q. Xu, C. Tian, X. Zhang, E. Plum, S. Zhang, J. Han, and W. Zhang, Optica **6**, 1190 (2019).
11. A. Pors, M. G. Nielsen, and S. I. Bozhevolnyi, Optica **2**, 716 (2015).
12. R. C. Devlin, A. Ambrosio, N. A. Rubin, J. P. B. Mueller, and F. Capasso, Science **358**, 896 (2017).
13. F. Yue, D. Wen, C. Zhang, B. D. Gerardot, W. Wang, S. Zhang, and X. Chen, Adv. Mater. **29**, 1603838 (2017).
14. F. Yue, C. Zhang, X. Zang, D. Wen, B. D. Gerardot, S. Zhang, and X. Chen, Light Sci. Appl. **7**, 17129 (2018).
15. X. Zang, F. Dong, F. Yue, C. Zhang, L. Xu, Z. Song, M. Chen, P. Y. Chen, G. S. Buller, Y. Zhu, S. Zhuang, W. Chu, S. Zhang, and X. Chen, Adv. Mater. **30**, 1707499 (2018).
16. X. Chen, M. Chen, M. Q. Mehmood, D. Wen, F. Yue, C. W. Qiu, and S. Zhang, Adv. Opt. Mater. **3**, 1201 (2015).
17. K. Ou, G. Li, T. Li, H. Yang, F. Yu, J. Chen, Z. Zhao, G. Cao, X. Chen, and W. Lu, Nanoscale **10**, 19154 (2018).
18. Z. Yang, Z. Wang, Y. Wang, X. Feng, M. Zhao, Z. Wan, L. Zhu, J. Liu, Y. Huang, J. Xia, and M. Wegener, Nat. Commun. **9**, 4607 (2018).
19. Z. Fan, H. Qiu, H. Zhang, X. Pang, L. Zhou, L. Liu, H. Ren, Q. Wang, and J. Dong, Light Sci. Appl. **8**, 67 (2019).
20. B. Yao, X. Zang, Z. Li, L. Chen, J. Xie, Y. Zhu, and S. Zhuang, Photonics Res. **8**, 830 (2020).
21. X. Zang, H. Ding, Y. Intaravanne, L. Chen, Y. Peng, J. Xie, Q. Ke, A. V. Balakin, A. P. Shkurinov, X. Chen, Y. Zhu, and S. Zhuang, Laser Photonics Rev. **13**, 1900182 (2019).
22. D. Wen, S. Chen, F. Yue, K. Chan, M. Chen, M. Ardron, K. F. Li, P. W. H. Wong, K. W. Cheah, E. Y. B. Pun, G. Li, S. Zhang, and X. Chen, Adv. Opt. Mater. **4**, 321 (2016).
23. Z. Zhang, D. Wen, C. Zhang, M. Chen, W. Wang, S. Chen, and X. Chen, ACS Photonics **5**, 1794 (2018).
24. D. Jia, Y. Tian, W. Ma, X. Gong, J. Yu, G. Zhao, and X. Yu, Opt. Lett. **42**, 4494 (2017).
25. Z. Shen, S. Zhou, S. Ge, W. Duan, L. Ma, Y. Lu, and W. Hu, Opt. Express **27**, 8800 (2019).
26. X. Jiang, H. Chen, Z. Li, H. Yuan, L. Cao, Z. Luo, K. Zhang, Z. Zhang, Z. Wen, L. Zhu, X. Zhou, G. Liang, D. Ruan, L. Du, L. Wang, and G. Chen, Opt. Express **26**, 14132 (2018).
27. H. Chen, Z. Wu, Z. Li, Z. Luo, X. Jiang, Z. Wen, L. Zhu, X. Zhou, H. Li, Z. Shang, Z. Zhang, K. Zhang, G. Liang, S. Jiang, L. Du, and G. Chen, Opt. Express **26**, 29817 (2018).
28. S. Wang, X. Wang, Q. Kan, J. Ye, S. Feng, W. Sun, P. Han, S. Qu, and Y. Zhang, Opt. Express **23**, 26434 (2015).
29. T. Zhou, J. Du, Y. Liu, and X. Zang, Opt. Lett. **45**, 463 (2020).
30. H. Zhao, X. Wang, J. He, J. Guo, J. Ye, Q. Kan, and Y. Zhang, Sci. Rep. **7**, 17882 (2017).
31. Q. Yang, J. Gu, Y. Xu, X. Zhang, Y. Li, C. Ouyang, Z. Tian, J. Han, and W. Zhang, Adv. Opt. Mater. **5**, 1601084 (2017).
32. X. Zang, W. Xu, M. Gu, B. Yao, L. Chen, Y. Peng, J. Xie, A. V. Balakin, A. P. Shkurinov, Y. Zhu, and S. Zhaung, Adv. Opt. Mater. **8**, 1901342 (2020).
33. N. Ullah, W. Liu, G. Wang, Z. Wang, A. U. R. Khalid, B. Hu, J. Liu, and Y. Zhang, Opt. Express **28**, 2789 (2020).
34. R. Wang, L. Li, H. Tian, J. Liu, J. Liu, F. Tian, J. Zhang, and W. Sun, Opt. Commun. **427**, 469 (2018).
35. X. Zang, H. Gong, Z. Li, J. Xie, Q. Cheng, L. Chen, A. P. Shkurinov, Y. Zhu, and S. Zhuang, Appl. Phys. Lett. **112**, 171111 (2018).
36. F. Ding, Z. Wang, S. He, V. M. Shalaev, and A. V. Kildishev, ACS Nano **9**, 4111 (2015).
37. D. Wen, F. Yue, S. Kumar, Y. Ma, M. Chen, X. Ren, P. E. Kremer, B. D. Gerardot, M. R. Taghizadeh, G. S. Buller, and X. Chen, Opt. Express **23**, 10272 (2015).
38. Y. Zhang, W. Liu, J. Gao, and X. Yang, Adv. Opt. Mater. **6**, 1701228 (2018).